Available online at www.sciencedirect.com
SCIENCE DIRECT
Polymer 46 (2005) 11978–11985
polymer
www.elsevier.com/locate/polymer

Isothermal crystallization of intercalated and exfoliated polyethylene/montmorillonite nanocomposites prepared by in situ polymerization

Jun-Ting Xu *, Yan-Qin Zhao, Qi Wang, Zhi-Qiang Fan

Department of Polymer Science and Engineering, Zhejiang University, Hangzhou 310027, China

Received 27 March 2005; received in revised form 19 July 2005; accepted 3 October 2005
Available online 26 October 2005

Abstract

Polyethylene/montmorillonite (PE/MMT) nanocomposites with different dispersion states of MMT were prepared by in situ polymerization. Isothermal crystallization of the intercalated nanocomposite, in which the PE chains were confined in the MMT layers, was studied and was compared with that of the exfoliated nanocomposite. It is observed that the intercalated sample has longer induction period, longer crystallization half time and larger crystallization activation energy than the exfoliated sample, showing that crystallization of PE is retarded due to confinement of the MMT layers. Analysis of crystallization kinetics shows that Avrami exponent (n) increases gradually with crystallization temperature. However, the maximal value of n is 2.0 for the intercalated sample, but it can reach 3.0 for the exfoliated sample. It is inferred that the stems of the PE crystals confined in the MMT layers are parallel to the MMT layers. The Hoffman–Weeks extrapolation method cannot be applied in the intercalated sample because of the small lateral surface of the PE crystals. Based on the depression of the melting temperature, the specific free energy of the PE/MMT interface was estimated, which is about 1.0 mJ/cm^2, much smaller than the free energy of the lateral surface of PE crystals. This is attributed to the origin of the strong nucleation effect of MMT.

Keywords: Polyethylene; Crystallization; Nanocomposite

1. Introduction

Polymer/clay nanocomposites usually have improved properties when compared to the neat polymers, such as better mechanical properties, higher thermal stability, reduced thermal expansion coefficients and gas permeability [1–10]. The clay can exist in the nanocomposites in two forms: intercalated and exfoliated. Melting blending and solution blending methods are frequently used for preparation of polymer/clay nanocomposites [11–22]. However, fully intercalated nanocomposites cannot be prepared through both ways and there are always lots of polymers outside the clay layers.

Polymer/nanocomposites can also be prepared by in situ polymerization, in which monomer and catalyst (or initiator) are loaded into the clay layers and polymerization takes place in the clay layers [23–33]. With the progress of polymerization, the d-spacing between clay layers increases gradually and the dispersion state of the clay changes from intercalation into exfoliation. As a result, if the amount of polymer polymerized in the clay layers is controlled at a low level, fully intercalated nanocomposite with few polymers outside the clay layers can be prepared. Such a nanocomposite provides a perfect model for study on behavior of polymer confined in a two-dimensional space [34,35]. For example, it has been revealed that crystallization of polymer is suppressed when the polymer chains are intercalated into the nano-galleries of the clay [36,37].

Moreover, crystalline polymer/clay nanocomposites have been well studied. It is observed that clay can greatly affect crystallization of polymer. The most frequently reported is nucleation effect of the clay [17,38–42]. The nucleation process involves polymer-clay interface and thus specific free energy of polymer-clay interface is an important parameter. However, to my best knowledge, so far there is few data of the specific free energy of polymer-clay interface reported [43–46].

In our previous work, ethylene polymerization was conducted using metallocene supported between the montmorillonite layers as catalyst [33]. By controlling the polymerization time (i.e. polymer content), both intercalated

* Corresponding author. Tel./fax: +86 571 87952400.
E-mail address: xujt@zju.edu.cn (J.-T. Xu).

0032-3861/$ - see front matter © 2005 Elsevier Ltd. All rights reserved.
doi:10.1016/j.polymer.2005.10.004

polyethylene/montmorillonite (PE/MMT) nanocomposite with few polymers outside the MMT layers and fully exfoliated PE/MMT nanocomposite were obtained [47]. In the present work, isothermal crystallization behavior of the intercalated nanocomposite, in which PE chains was confined between the MMT layers, was studied and was compared with that of the exfoliated nanocomposite.

2. Experimental

2.1. Preparation and characterization of the PE/MMT nanocomposites

Details of preparation and characterization of the nanocomposites have been described in Ref. [33]. Sodium montmorillonite (Na-MMT) was purchased from the Zhejiang Huate Company, China. Its specific surface is 700 m^2/g, and the cation-exchange capacity is 90 mmol/g. The clay was purified according to standard sedimentation methods and dried under vacuum at 200 °C overnight. The catalyst intercalated inorganic montmorillonite was prepared in the following procedures. 0.87 g of inorganic MMT was treated with 4 mL of methyl aluminoxane (MAO) solution (10 w/v% in toluene) at 50 °C in 20 mL of toluene (refluxed and distilled under argon with sodium benzophenone ketyl as indicator) for 4 h, followed by washing with 3×20 mL of dry toluene. Then 20 mg of $(n\text{-Bu-Cp})_2ZrCl_2$ in 20 mL of toluene was added to the treated MMT and kept at 50 °C for 4 h, followed by washing with 3×20 mL of dry toluene. After drying under vacuum for 6 h, the intercalated MMT, named Zr-MMT, was obtained. Ethylene polymerization was conducted in a 100-mL flask equipped with an ethylene inlet and a magnetic stirrer. At first 0.18 g of Zr-MMT and 50 mL of toluene were added. After the toluene was saturated with ethylene of 1 atm pressure, 1.0 mL of MAO solution was injected to initiate the polymerization at 50 °C. The polymerization was terminated by the addition of acidified ethanol, and the polymer was washed with ethanol and dried in vacuum oven at 50 °C. By control of polymerization time, two composite samples, namely intercalated sample and exfoliated sample, were prepared. The content of PE in the nanocomposites were determined by extraction with xylene, and the xylene-extractable polyethylene was subjected to gel permeation chromatography (GPC) characterization, which was performed on a PL GPC-220 in 1,2,4-trichlorobenzene at 150 °C using narrow polystyrene as the standard. XRD analyses were performed using a Siemens D5000 diffractometer with Cu radiation (40 kV, 40 mA). Scanning was in 0.02° steps at a speed of 2°/min. Transmission electron microscopy (TEM) micrographs were obtained with a JEM-1230 using an acceleration voltage of 120 kV.

2.2. DSC experiments

DSC experiments were carried out in a Perkin–Elmer Pyris-1instrument. About 4–5 mg of the sample was encapsulated in an aluminum pan. The samples were first kept at 200 °C for 5 min to erase the thermal history, then were cooled to pre-set temperature at cooling rate of 100 °C/min to conduct isothermal crystallization. After crystallization, the samples were heated to melt at a rate of 10 °C/min.

3. Results and discussion

3.1. Structure of PE/MMT nanocomposites

Before discussing the structure of PE/MMT nanocomposites, preparation of the MMT-supported catalyst is briefly introduced. The MMT was first treated with MAO, which can react with residual water existing between the MMT layers. Then the metallocene catalyst added reacts with the supported MAO to form ion pairs, in which the metallocene forms the cation and MAO forms the anion. As a result, the catalyst can be easily loaded into the MMT galleries though the MMT is hydrophilic. The metallocene physically absorbed onto the MMT was removed by repeated washing until no metallocene is detected in the solution. The WAXD patterns of Zr-MMT and the PE/MMT nanocomposites prepared at different polymerization times (t_p) are shown in Fig. 1. It is found that after immobilization of catalyst on MMT, the (001) WAXD peak of MMT becomes diffused, as compared with the sharp peak of neat MMT [33]. This also shows that the catalyst is loaded into the MMT galleries, leading to the irregular *d*-spacing between the MMT layers. Fig. 2 shows the TEM micrographs of the PE/MMT nanocomposites. It is found that in the nanocomposite prepared at $t_p = 15$ min the MMT layers aggregate seriously. Since MMT is dark in TEM observation, only image of low magnification is obtained for this sample and the *d*-spacing between the MMT layers cannot be determined by TEM and can only be calculated from its WAXD pattern. However, the aggregated morphology can be viewed as indirect evidence that few polymers exist outside the MMT

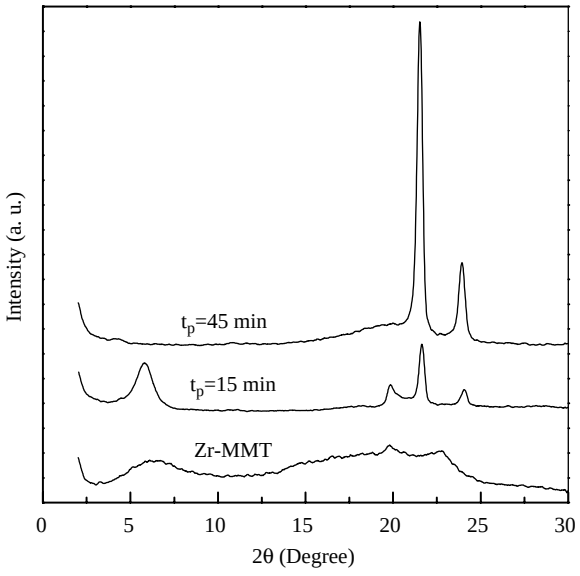

Fig. 1. WAXD patterns of Zr-MMT(supported catalyst) and the PE/MMT nanocomposites obtained at different polymerization times (t_p).

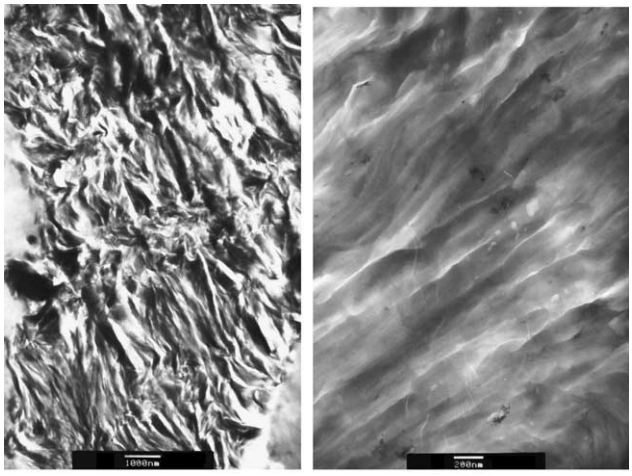

Fig. 2. TEM micrographs of the PE/MMT nanocomposites obtained at different polymerization times (t_p). (a) $t_p = 15$ min, the scale bar is 1000 nm; (b) $t_p = 45$ min, the scale bar is 200 nm.

layers. The MMT layers are not very clear in the sample prepared at $t_p = 45$ min either because all MMT has been exfoliated into thin layers by PE. However, we still can see some regular lamellar structure and the *d*-spacing is about 10–20 nm. Table 1 summarizes polymerization time, polyethylene content, molecular weight and molecular weight distribution of the PE/MMT nanocomposites. These two samples were prepared with the sample catalyst but at different polymerization times, thus the content of MMT in the nanocomposites can be regulated. One can see from Fig. 1 that after polymerization for 15 min, the lamellar structure of the MMT is still retained, but the *d*-spacing between the MMT layers becomes a little larger, as compared to that of Zr-MMT. This shows that PE is produced between the MMT layers and thus increases the *d*-spacing. In contrast, after polymerization for 45 min, the content of PE in the PE/MMT nanocomposite is increased and the (001) reflection from MMT basically disappears, indicating that the MMT layers are exfoliated. Molecular weight is another important evidence supporting that polymerization proceeds in the MMT galleries at shorter polymerization time. The data in Table 1 shows that the sample obtained at $t_p = 15$ min has higher molecular weight than the sample obtained at $t_p = 45$ min, though the former was prepared at much shorter polymerization time. Because polymerization proceeds in the MMT galleries, the rate of chain transfer is greatly reduced, which results in high molecular weight PE.

Table 1
Polymerization time, polyethylene content, molecular weight and molecular weight distribution of PE/MMT nanocomposites

	Polymerization time (min)	MMT content (wt%)	M_n	M_w/M_n
Intercalated sample	15	23	6.7×10^4	3.3
Exfoliated sample	45	11	4.4×10^4	2.6

After exfoliation of the MMT layers, the active sites are more exposed to chain transfer reagent and the product has lower molecular weight. Therefore, we can obtain completely intercalated PE/MMT nanocomposite with few PE located outside the MMT layers and exfoliated PE/MMT sample by in situ polymerization.

3.2. Isothermal crystallization kinetics

Fig. 3 shows the heat flow curves of these two nanocomposites during isothermal crystallization and the plots of relative crystallinity ($X(t)$) versus crystallization time (t) at various crystallization temperatures (T_c) are shown in Fig. 4. For the purpose of comparison, the curves at $T_c = 125.8$ °C in Fig. 4(a) and (b) are compiled together and shown in Fig. 5. One can see from Fig. 5 that at the same crystallization temperature the crystallization rate of the intercalated sample is slower than that

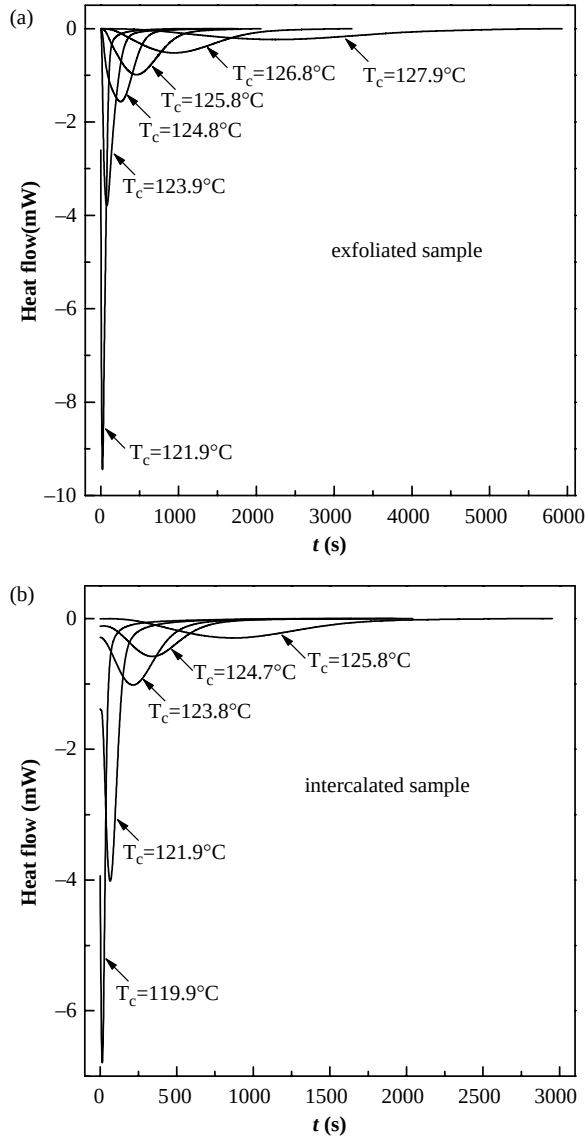

Fig. 3. Heat flow curves of PE/MMT nanocomposites during isothermal crystallization. (a) Exfoliated sample; (b) intercalated sample.

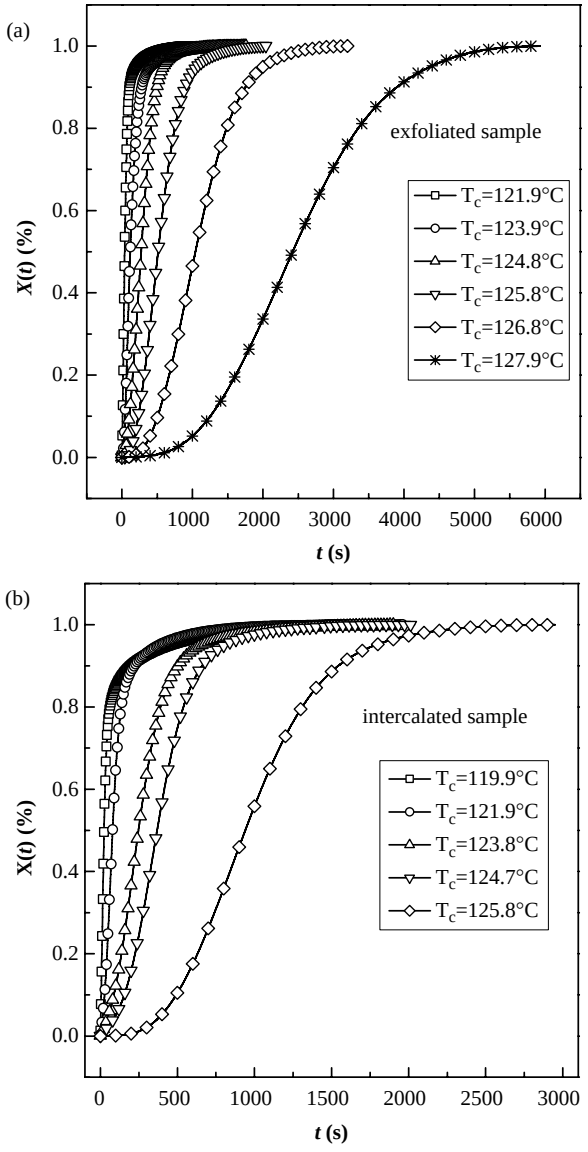

Fig. 4. Plots of relative crystallinity versus crystallization time at various crystallization temperatures. (a) Exfoliated sample; (b) intercalated sample.

of the exfoliated sample. Moreover, it is observed that crystallization starts immediately in the exfoliated sample when crystallization temperature reaches, while there is an induction period for the intercalated sample. Fig. 6 illustrates crystallization half time of these two nanocomposites. It is found that at the same crystallization temperature the intercalated sample has longer crystallization half time than the exfoliated sample, indicating slower crystallization rate. These findings are in accordance with our results of non-isothermal crystallization [48]. In non-isothermal crystallization we found that crystallinity of the intercalated sample increases very slowly in the initial period of crystallization, though the onset crystallization temperature of the intercalated sample is higher due to the stronger nucleation effect of the MMT in this sample [48]. The slower crystallization rate of the intercalated sample is mainly due to the confinement effect of

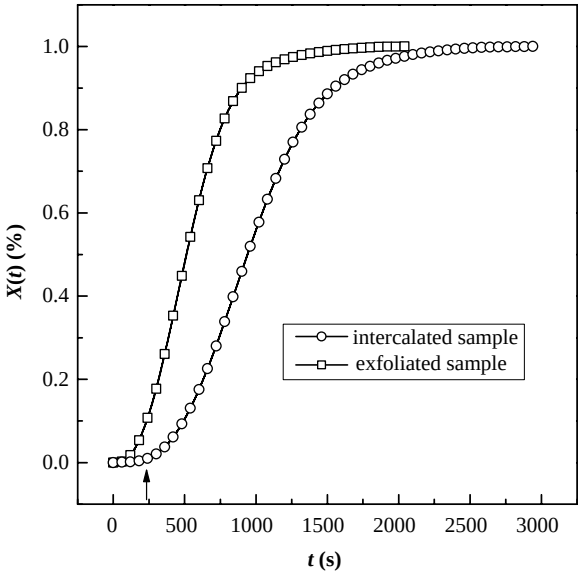

Fig. 5. Comparison of the $X(t)$–t curves of the intercalated and exfoliated sample at $T_c = 125.8\,^{\circ}C$. The arrow indicates the induction period of the intercalated sample.

the MMT layers, but the higher molecular weight of this sample may also play a minor role.

The isothermal crystallization kinetics of the PE/MMT nanocomposites was treated with Avrami equation [49]:

$$1 - X(t) = \frac{\Delta H^c_{t=\infty} - \Delta H^c_t}{\Delta H^c_{t=\infty} - \Delta H^c_{t=0}} = \exp(-Kt^n) \quad (1)$$

Where $X(t)$ is the relative crystallinity at time t, $\Delta H^c_{t=\infty}$ and ΔH^c_t are the crystallization enthalpies on complete crystallization and after time t. Therefore, we have:

$$\ln[-\ln(1 - X(t))] = \ln K + n \ln t \quad (2)$$

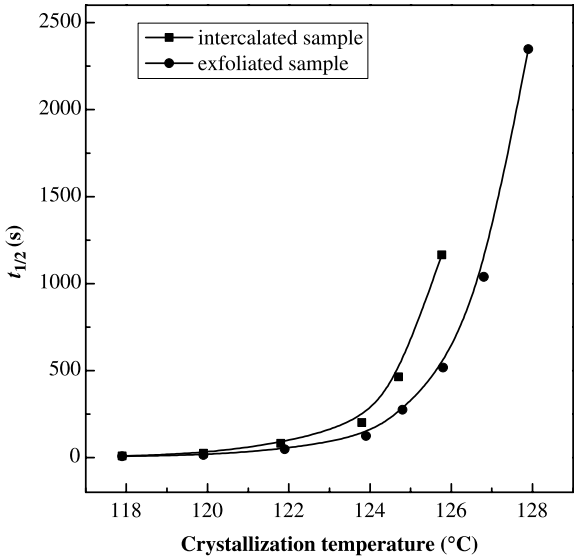

Fig. 6. Crystallization half time of the exfoliated sample and the intercalated sample at various crystallization temperatures.

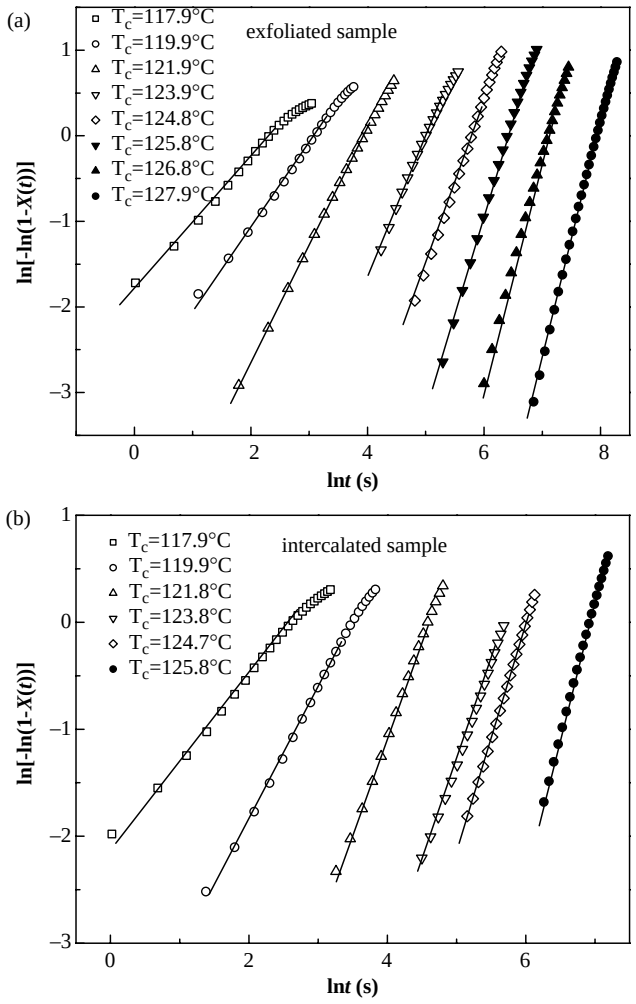

Fig. 7. Avrami plots of the exfoliated sample (a) and the intercalated sample (b) at various crystallization temperatures.

The crystallization rate constant K and Avrami exponent n can be determined from the intercept and slope in the plot of $\ln[-\ln(1-X(t))]$ versus $\ln(t)$.

Fig. 7 shows the Avrami plots of the intercalated and exfoliated PE/MMT nanocomposites at various crystallization temperatures. The values of n and $\ln K$ are shown in Figs. 8 and 9, respectively. It is observed that Avrami exponent increases with crystallization temperature, and $\ln K$ decreases with crystallization temperature for both the exfoliated and intercalated samples. This phenomenon is similar to that observed for neat polyethylene [29,50]. However, we notice that the maximal value of n for the intercalated sample is around 2.0, indicating two-dimensional growth of PE crystals in this sample. In contrast, the Avrami exponent of the exfoliated sample can reach 3.0 at high crystallization temperature, showing three-dimensional growth of PE crystals. The Avrami exponents of these two nanocomposites are in accordance with their structure. In the intercalated sample polymer chains are confined in the MMT layers and only two-dimensional PE crystals are formed, while spherulites can be formed in the exfoliated sample. Considering the smaller

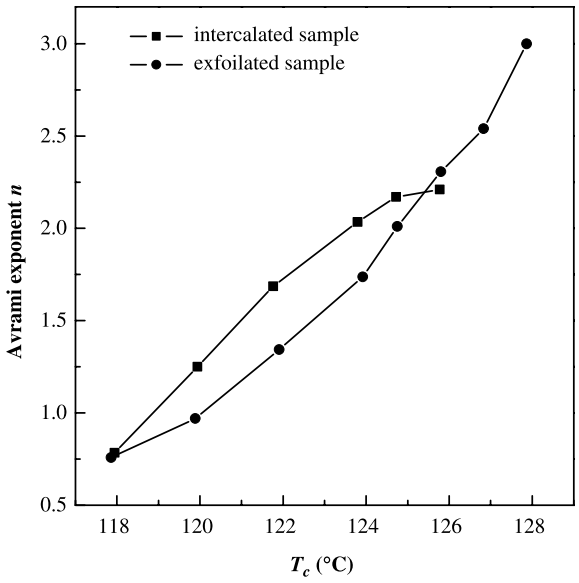

Fig. 8. Avrami exponents at various crystallization temperatures.

d-spacing between the MMT layers and the melting temperature just slightly lower than that of neat PE, we can conclude that the PE stems in the intercalated sample are parallel to the MMT layers, but not perpendicular to the clay layers, as shown in Fig. 10. Otherwise, if the PE stems are perpendicular to the MMT layers, the lamellar thickness of PE crystals is comparable to the d-spacing of the MMT layers and thus the PE crystals will have a much lower melting temperature.

The crystallization rate constant K can be approximately described by an Arrhenius equation:

$$K^{1/n} = K_0 \exp\left(\frac{-\Delta E}{RT_c}\right) \tag{3}$$

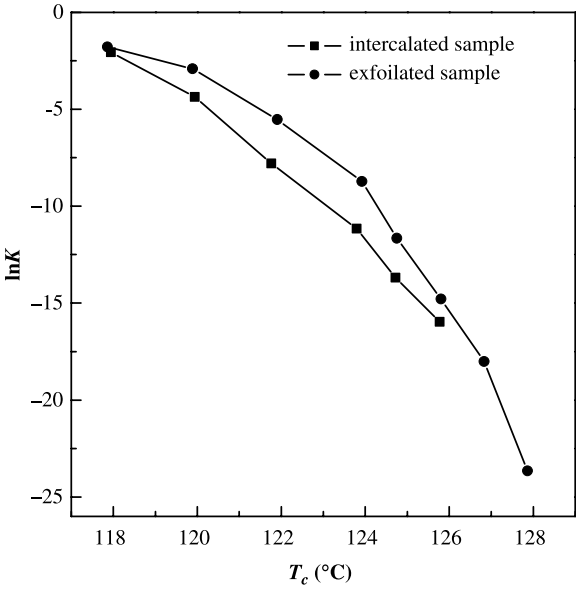

Fig. 9. The values of $\ln K$ at various crystallization temperatures.

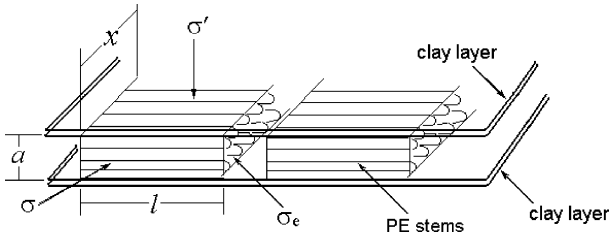

Fig. 10. Schematic of PE crystals in the intercalated sample.

where K_0 is a pre-exponential factor, R is the universal gas constant, and ΔE is the activation energy.

The value of the activation energy for the primary crystallization process was calculated from the plot of $(1/n)\ln K$ versus T_c (Fig. 11). It is observed that the Arrhenius plots are linear only at higher crystallization temperatures for both samples. The values of ΔE are 139.6 and 111.8 kJ/mol for the intercalated and the exfoliated sample. The crystallization activation energy is the sum of the transport activation energy and the nucleation activation energy. As mentioned above, the nucleation effect of the MMT on crystallization of PE is stronger in the intercalated sample, as indicated by its higher onset crystallization temperature in non-isothermal crystallization [48]. Therefore, we believe that the larger crystallization activation energy of the intercalated sample originates from its higher transport activation energy, because the PE chains are confined between the MMT layers and have poor mobility.

3.3. Equilibrium melting temperature

The melting temperature of a polymer crystal with infinite lateral size can be expressed by Thomson–Gibson equation:

$$T_m = T_m^0\left(1-\frac{2\sigma_e}{l\Delta H_f}\right) \tag{4}$$

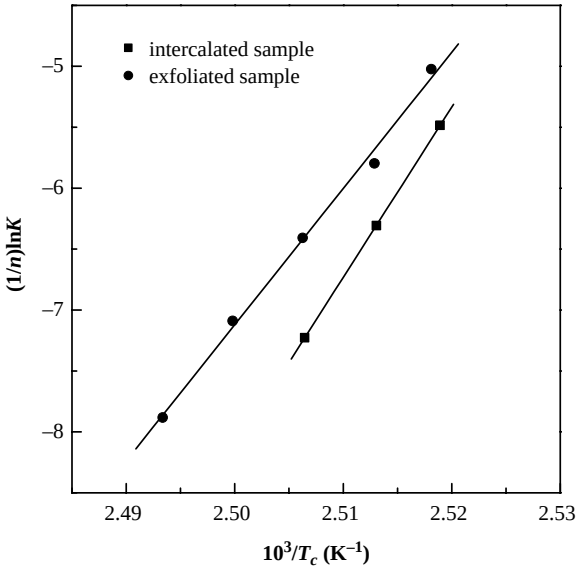

Fig. 11. Plots of $(1/n)\ln K$ versus $1/T_c$.

Where T_m and T_m^0 are the melting temperature and equilibrium melting temperature, respectively. σ_e is the free energy of the folding surface, l is the lamellar thickness of polymer crystals, and ΔH_f is the fusion enthalpy per unit volume.

Based on Eq. (4), Hoffman and Weeks derived the melting temperature of polymer crystals with infinite lateral size [51]:

$$T_m = \left(1-\frac{1}{\gamma}\right)T_m^0 + \frac{T_c}{\gamma} \tag{5}$$

where γ is the ratio of the crystal thickness to the thickness of the initial nucleus at the crystallization temperature T_c, and γ is equal to

$$\gamma = \frac{l\Delta H_f(T_m^0 - T_c)}{2\sigma_e T_m^0} \tag{6}$$

When the plot of melting temperature versus crystallization temperature is extrapolated to $T_c = T_m = T_m^0$, the equilibrium melting temperature of polymer crystals with infinite lateral size can be obtained.

The Hoffman–Weeks plots for these two samples are illustrated in Fig. 11. It is found that the value of T_m^0 is 144.7 °C for the exfoliated sample, which is very close to the values reported for the neat linear polyethylene. Nevertheless, the value of extrapolated T_m^0 for the intercalated sample is only 142.5 °C. Although the difference is only 2 °C, we found that at the same crystallization temperature the melting temperature of the intercalated sample is systematically lower than that of the exfoliated sample.

There are two possibilities: (1) The intercalated sample has lower equilibrium melting temperature than the exfoliated sample. (2) The Hoffman–Weeks extrapolation is not applicable to the intercalated sample. Since the exfoliated sample has the same equilibrium melting temperature as the neat PE, we believe that addition of MMT to PE doesnot affect T_m^0 of PE and the second case is the real situation of the intercalated nanocomposite. The reason for inapplicability of Hoffman–Weeks extrapolation is that the PE crystals in the intercalated sample have two small lateral surfaces and the Hoffman–Weeks equation is only applicable to the polymer crystals with infinite lateral size.

For the PE crystals shown in Fig. 10, we have:

$$\Delta G = 2xl\sigma' + 2al\sigma + 2ax\sigma_e - alx(\Delta F) \tag{7}$$

Where ΔG is the free energy for formation of a crystal, ΔF is the free energy difference between the supercooled liquid phase and the bulk crystal phase, l is the lamellar thickness of PE crystals, a and x are the lateral sizes of PE crystals, in which a is equal to the d-spacing of MMT layers. σ_e, σ and σ' are the specific free energies of the folding surface, the lateral surface and the PE-MMT interface, respectively. The expression of ΔF can be approximately written as:

$$\Delta F = \Delta H_f - T_m\Delta S_f = \Delta H_f - \frac{T_m\Delta H_f}{T_m^0} \tag{8}$$

While melting, ΔG is equal to 0, then the melting temperature of PE crystals with thickness of l is:

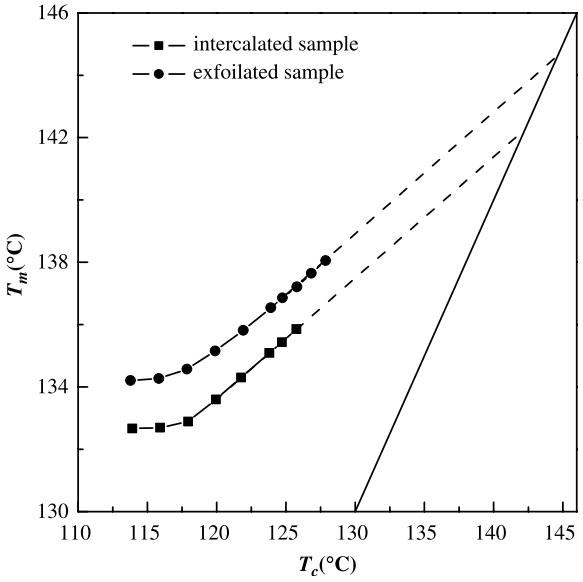

Fig. 12. Hoffman–Weeks plots for the intercalated and exfoliated samples.

$$T_m = T_m^0\left[\frac{1-((2\sigma'/a)+(2\sigma/x)+(2\sigma_e/l))}{\Delta H_f}\right] \quad (9)$$

When the PE crystals are confined between the MMT layers with PE stems parallel to the MMT layers, the value of x is quite large, but the parameters a and l have smaller values. The melting temperature of PE crystals is:

$$T_m = T_m^0\left[\frac{1-((2\sigma'/a)+(2\sigma_e/l))}{\Delta H_f}\right] \quad (10)$$

Comparing Eqs. (4) and (10), one can see that the lower melting temperature of the intercalated sample is due to the smaller lateral surface perpendicular to the MMT layer. The free energy of the PE-MMT interface can be estimated from the depression of the melting temperature. As shown in Fig. 12, the melting temperature of the intercalated sample is about 2 °C lower than that of the exfoliated sample when it is extrapolated to $T_m = T_c$ ($l = \infty$). Thus we have:

$$2 = \frac{2T_m^0\sigma'}{(a\Delta H_f)} \quad (11)$$

and

$$\sigma' = \frac{a\Delta H_f}{T_m^0} \quad (12)$$

The values of ΔH_f and T_m^0 are 2.80×10^8 J/m^3 and 417.7 K, respectively [52]. The parameter a is 15.2 Å, which is determined from the d-spacing of the MMT (Fig. 1). It is found that the free energy of the PE-MMT interface σ' is only 1.0 mJ/m^2, which is much smaller than σ (11.8 mJ/m^2) for the lateral surface and σ_e ($\sim$100 mJ/m^2) for the folding surface of PE crystals [52].

For heterogeneous nucleation process, we have [53]:

$$\Delta G = -a'x'l'\Delta F + x'l'\Delta\sigma + 2a'l'\sigma + 2a'x'\sigma_e \quad (13)$$

where a', x' and l' are the dimension of the nucleated polymer crystal embryo, respectively. $\Delta\sigma$ is the specific interfacial free energy difference accounting for one surface contacting the melt (of surface free energy $x'l'\sigma$) and one surface contacting the heterogeneous nucleus. The expression of $\Delta\sigma$ is [54]:

$$\Delta\sigma = \sigma + \sigma' - \sigma'' \quad (14)$$

where σ, σ' and σ'' are the specific interfacial free energies of crystal-melt, crystal-substrate and melt-substrate interfaces, respectively.

While for homogeneous nucleation process, we have [54]:

$$\Delta G = -a'x'l'\Delta F + 2x'l'\sigma + 2a'l'\sigma + 2a'x'\sigma_e \quad (15)$$

Comparing Eqs. (13) and (15), one can see that, if $\Delta\sigma$ is smaller than 2σ, heterogeneous nucleation is preferred. We have known that σ' is much smaller than σ and σ'' is positive, so $\Delta\sigma$ is actually smaller than 2σ. As a result, the smaller specific free energy of PE-MMT interface is the origin of the stronger nucleation ability of MMT.

4. Conclusion

Isothermal crystallization of the PE/MMT nanocomposites shows that confinement of MMT layers retards crystallization of PE chains, leading to longer induction period, longer crystallization half time and larger crystallization activation energy. Avrami analysis implies that the growth of PE crystals in the intercalated sample is two-dimensional and the PE stems are parallel to the MMT layers. Because of the smaller lateral surface of the PE crystals confined in the MMT layers, the intercalated sample has lower melting temperature. Based on the depression of melting temperature, the specific free energy of the PE-MMT interface was estimated. It is found that the specific free energy of the PE-MMT interface is much smaller than those of the lateral surface and folding surface of PE crystals.

Acknowledgements

This work was supported by the State Key Fundamental Research Project of China (Grant G1999064801).

References

[1] Oberdisse J. Macromolecules 2002;35:9441.
[2] Yeh JM, Chen CL, Chen YC, Ma CY, Lee KR, Wei Y, et al. Polymer 2002;43:2729.
[3] Gopakumar TG, Lee JA, Kontopoulou M, Parent JS. Polymer 2002;43:5483.
[4] Ray SS, Okamoto M. Macromol Rapid Commun 2003;24:815.
[5] Khayankarn O, Magaraphan R, Schwank JW. J Appl Polym Sci 2003;89:2875.
[6] Cypes SH, Saltzman WM, Giannelis EP. J Controlled Release 2003;90:163.
[7] Chang JH, An YU, Cho DH, Giannelis EP. Polymer 2003;44:3715.
[8] Shah D, Maiti P, Gunn E, Schmidt DF, Jiang DD, Batt CA, et al. Adv Mater 2004;16:1173.
[9] Chen W, Feng L, Qu BJ. Solid State Commun 2004;130:259.

[10] He AH, Hu HQ, Huang YJ, Dong JY, Han CC. Macromol Rapid Commun 2004;25:2008.
[11] Liang GD, Xu JT, Xu WB. J Appl Polym Sci 2004;91:3054.
[12] Liang GD, Xu JT, Bao SP, Xu WB. J Appl Polym Sci 2004;91:3974.
[13] Park CI, Park OO, Lim JG, Kim HJ. Polymer 2001;42:7465.
[14] Nam PH, Maiti P, Okamoto M, Kotaka T, Hasegawa N, Usuki A. Polymer 2001;42:9633.
[15] Nam JY, Ray SS, Okamoto M. Macromolecules 2003;36:7126.
[16] Kalgaonkar RA, Jog JP. J Polym Sci, Part B: Polym Phys 2003;41:3102.
[17] Pozsgay A, Frater T, Papp L, Sajo I, Pukanszky B. J Macromol Sci, Phys 2002;B41:1249.
[18] Priya L, Jog JP. J Polym Sci, Part B: Polym Phys 2003;41:31.
[19] Chang JH, Jang TG, Ihn KJ, Lee WK, Sur GS. J Appl Polym Sci 2003;90: 3208.
[20] Xu WB, Liang GD, Zhai HB, Tang SP, Hang GP, Pan WP. Eur Polym J 2003;39:1467.
[21] Phang IY, Pramoda KP, Liu TX, He CB. Polym Int 2004;53:1282.
[22] Liao MY, Zhu JD, Xu HD, Li Y, Shan W. J Appl Polym Sci 2004;92: 3430.
[23] Tudor J, Ohare D. Chem Commun 1997;603.
[24] Weimer MW, Chen H, Giannelis EP, Sogah DY. J Am Chem Soc 1999; 121:1615.
[25] Heinemann J, Reichert P, Thomann R, Mulhaupt R. Macromol Rapid Commun 1999;20:423.
[26] Jin YH, Park HJ, Im SS, Kwak SY, Kwak S. Macromol Rapid Commun 2002;23:135.
[27] Ke YC, Long CF, Qi ZN. J Appl Polym Sci 1999;71:1139.
[28] Imai Y, Inukai Y, Tateyama H. Polym J 2003;35:230.
[29] Kuo SW, Huang WJ, Huang SB, Kao HC, Chang FC. Polymer 2003;44: 7709.
[30] Yang F, Zhang XQ, Zhao HC, Chen B, Huang BT, Feng ZL. J Appl Polym Sci 2003;89:3680.
[31] Kiersnowski A, Piglowski J. Eur Polym J 2004;40:1199.
[32] Yu YH, Yeh JM, Liou SJ, Chen CL, Liaw DJ, Lu HY. J Appl Polym Sci 2004;92:3573.
[33] Wang Q, Zhou ZY, Song LX, Xu H, Wang L. J Polym Sci, Part A: Polym Chem 2004;42:38.
[34] Giannelis EP, Krishnamoorti R, Manias E. Adv Polym Sci 1999;138:107.
[35] Manias E, Chen H, Krishnamoorti R, Genzer J, Kramer EJ, Giannelis EP. Macromolecules 2000;33:7955.
[36] Kuppa V, Menakanit S, Krishnamoorti R, Manias E. J Polym Sci, Part B: Polym Phys 2003;41:3285.
[37] Waddon AJ, Petrovic ZS. Polym J 2002;34:876.
[38] Ou CF. J Polym Sci, Part B: Polym Phys 2003;41:2902.
[39] Ou CF, Ho MT, Lin JR. J Polym Res-Taiwan 2003;10:127.
[40] Ma JS, Zhang SM, Qi ZN, Li G, Hu YL. J Appl Polym Sci 2002;83:1978.
[41] Ke YC, Yang ZB, Zhu CF. J Appl Polym Sci 2002;85:2677.
[42] Liu XH, Wu QJ, Berglund LA. Polymer 2002;43:4967.
[43] Lewin M, Mey-Marom A, Frank R. Polym Adv Technol 2005;16:429.
[44] Chen B, Evans JRG. Philos Mag 2005;85:1519.
[45] Lewin M. Fire Mater 2003;27:1.
[46] Park SJ, Seo DI, Lee JR. J Colloid Interface Sci 2002;251:160.
[47] Xu JT, Zhao YQ, Wang Q, Fan ZQ. Macromol Rapid Commun 2005;26: 620.
[48] Xu JT, Wang Q, Fan ZQ. Eur Polym J. 2005;41:3011.
[49] Avrami M. J Chem Phys 1939;7:1103.
[50] Janimak JJ, Stevens GC. Thermochim Acta 1999;332:125.
[51] Hoffman JD, Weeks JJ. J Res Natl Bur Stand 1962;66A:13.
[52] Mark JE, editor. Polymer data handbook. Oxford: Oxford University Press; 1999.
[53] Binsbergen FL. J Polym Sci, Part B: Polym Phys 1973;11:117.
[54] Wunderlich B. Macromolecular Physics. Crystal nucleation, growth, annealing. vol. 2. London: Academic Press; 1976.